Main Manuscript for

Neurons, Muscles, and Venom: Identifying Drivers of Cephalopod Predation

Kim N. Kirchhoff [1], José Ramón Pardos-Blas [2], Amy Courtney [3], Belkes Stambouli [1], Andrew L. Sugarman [4], Daniel J. Vanselow [4], Melvin Williams [1], Christian Carrasco [1], Mariam Gelashvili [1], Cecilia Cuddy [5], Praveena Naidu [1,7], William R. Schafer [3,6], Keith C. Cheng [4], Eve Seuntjens [6], Mandë Holford [1,7,8,*]

[1] Department of Organismic and Evolutionary Biology, Harvard University, Cambridge, MA, USA
[2] Department of Chemistry, Hunter College, CUNY, NY, USA
[3] MRC Laboratory of Molecular Biology, Cambridge, United Kingdom
[4] Department of Pathology, Pennsylvania State University College of Medicine, Hershey, PA, USA; Institute for Computational and Data Sciences, Pennsylvania State University, University Park, PA, USA
[5] Laboratory of Molecular Biology, The Rockefeller University, NYC, NY, USA
[6] Department of Biology, KU Leuven, Leuven, Belgium
[7] Programs in Biology, Biochemistry, and Chemistry at CUNY Graduate Center, NYC, NY, USA
[8] Department of Invertebrate Zoology, The American Museum of Natural History, NYC, NY, USA

* Correspondence: mholford@fas.harvard.edu

Author Contributions: conceptualization, M.H. and K.N.K.; methodology, M.H., E.S., A.C., K.C., A.L.S., D.J.V., J.R.P.B., C.Ca., P. N., C.C. and M.W.; validation, M.H., E.S., A.C., K.C., A.L.S., D.J.V., J.R.P.B., C.Ca., C.C. and M.W.; formal analysis, K.N.K., M.H., E.S., A.C., K.C., A.L.S., D.J.V., J.R.P.B., C.Ca., C.C. and M.W.; investigation, K.N.K., M.H., E.S., A.C., K.C., A.L.S., D.J.V., J.R.P.B., C.Ca., P. N., C.C. and M.W.; resources, K.N.K. and M.H.; data curation, K.N.K, B.S., A.M., K.C., A.L.S., D.J.V., J.R.P.B., P. N., C.C. and M.W.; writing-original draft preparation, K.N.K, B.S., M.H. and M.W.; writing-review and editing, K.N.K., B.S., M.H., E.S., A.C., K.C., A.L.S., D.J.V., J.R.P.B., C.Ca., C.C. and M.W.; visualization, K.N.K., A.C., K.C., A.L.S., D.J.V., J.R.P.B., C.Ca., C.C. and B.S.; supervision, M.H.; project administration, M.H.; funding acquisition, M.H. All authors have read and agreed to the published version of the manuscript.

Competing Interest Statement: The authors declare no competing interests.

Classification: Biological Sciences: Cell Biology and Neuroscience.

Keywords: Cephalopods, Venom gland, Neuronal control, Secretion

Abstract

Venom plays a central role in the predatory ecology of coleoid cephalopods (octopuses, squids, and cuttlefish), yet the mechanisms governing venom release from the posterior salivary gland (PSG) are unknown. Using a multimodal approach combining histology, *in situ* hybridization, comparative phylogenetics, and live imaging across multiple coleoid species, we characterize the structural and neuronal regulatory organization of the PSG. We show that the gland comprises two distinct tubular systems: secretory tubules specialized for venom production and smooth–striated tubules positioned to facilitate venom transport toward the beak for injection into its prey. Molecular localization of filamentous and α-actin confirms a circular smooth muscle layer surrounding the tubules. Mapping of six neuronal markers, including neurofilament (NF-H), synapsin, and muscle-type nicotinic acetylcholine receptors, reveals dense and stereotyped neural innervation closely associated with the muscular compartments. Comparative phylogenetic analyses of cys-loop ligand-gated ion channel sequences indicate a predominancy of excitatory acetylcholine- and dopamine-gated receptors in coleoid venom glands, implicating potential molecular agents involved in neural control of venom release. Consistent with neural regulation, *ex vivo* stimulation of the PSG elicits calcium signaling throughout the gland. Together, our results reveal a conserved venom gland structure among octopuses, squids, and cuttlefish, with a spatially distinct neuromuscular tissue organization indicating venom production and release sites modulated by a network of neuronal agents. This work provides a mechanistic framework into venom gland organization and molecular regulation of venom release in one of the oldest venomous lineages.

Significance Statement

Coleoid cephalopods (octopuses, squids, and cuttlefish) are predominantly known for their camouflage abilities and less for their use of venom in prey capture, defense, and sexual competition. How cephalopods release their venoms remains an open question. Our results indicate that the venom gland is differentiated into venom production and release tubular sections This bifurcation is conserved across several taxa including the longfin inshore squid, the hummingbird bobtail squid, and the California two-spot octopus, with few lineage-specific variations. Spatial molecular mapping revealed smooth muscle components and cholinergic neurons in intimate association with gland tubules. Comparative phylogenetic analyses further enhance neuronal network understanding by transcriptionally identifying conserved nicotinic acetylcholine-gated channels, divergent dopamine-gated channels, and multiple orphan ligand-gated ion channels with potentially novel functional properties. Our findings provide a comprehensive characterization of the network of molecular and neuronal components that can act in concert to facilitate cephalopod venom release. Future expansion and refinement of these results will enable mapping of the brain–bite neural circuit underlying cephalopod predation.

Introduction

Mollusks are the second-largest animal phylum, within which cephalopods (approximately 800 species) stand out for their complex cognition, camouflage, and highly developed central brain (1,2). Although these traits have attracted substantial research attention, cephalopod's use of venom for predation, defense and sexual competition is understudied. Venoms are complex biochemical cocktails—often composed of small molecules, peptides, and proteins—that have convergently evolved across major animal lineages (3,4) and have demonstrated therapeutic relevance (5). Despite the prevalence of venom in nature, the mechanisms underlying its biological processes such as production, regulation and release are not well understood.

Marine venomous organisms like cnidarians (*e.g.,* jellyfish) and coleoid cephalopods (octopuses, squids, cuttlefish) comprise some of the oldest venomous creatures dating back 500 million years (6) (Fig. 1a). A coleoid's specialized venom system consists of the posterior salivary gland (PSG), which can be single (in myopsid squids) or paired (in sepiolid squids, cuttlefish and octopuses), and is hypothesized to be the primary venom producing tissue (Fig. 1b). In the PSG, venom is stored in secretory granules that are released to the salivary papilla via the salivary duct, ultimately entering the buccal mass to enable immobilization of the prey (7,8) (Fig. 1b-e and Fig. S1).

However, the mechanism(s) controlling venom secretion remains unanswered. Prior morphological and histological studies in octopus from Young in the 1960's suggest venom release is controlled by dual innervation of the PSG (7,9). Specifically, it has been proposed that the superior buccal lobe innervates the basal membrane in the secretory tubules of the gland, while the fibers of the subradular ganglion regulate the smooth muscles in the gland and those associated with the salivary duct and papilla (7,9,10). However, molecular aspects of the venom release mechanism characterizing neuronal subtypes, neurotransmitter systems and signaling pathways have not been identified in any single species or in a broader comparative framework across the phylogenetic tree of cephalopods.

Here, we address these gaps in knowledge of venom release through comprehensive histological profiling of the neuronal and muscular molecular organization of PSGs across all three venomous coleoid cephalopod lineages: octopus - the California two-spot octopus (*Octopus bimaculoides*), squid - the longfin inshore squid (*Doryteuthis pealeii*, myopsid squid) and the hummingbird bobtail squid (*Euprymna berryi*, sepiolid squid), and cuttlefish - the dwarf cuttlefish (*Ascarosepion bandense*) and the common cuttlefish (*Sepia officinalis*) (Fig. 1a,b, Table S1). We use tissue-specific markers and *ex vivo* live staining recordings to identify key molecular components of muscular and neuronal tissue, analyze their distribution patterns from pre- to postsynaptic sites, and integrate them into a mapping of the potential neuronal signaling pathway. Additionally, we performed a phylogenetic analysis for a key ligand-gated ion channel family involved in synaptic transmission across metazoan taxa to identify the presence of homologous channels in the PSG of cephalopods.

By integrating structural, cellular, neuromuscular signals and channel homology between the more studied octopus (Octopodidae) and squids and cuttlefish (loliginid/sepiolid), we provide the first cross-species integrative comparison and neuromuscular characterization of coleoid venom glands. Our findings allow insights into the nerve subtypes and neurotransmitters that may regulate coleoid venom release, elucidating spatial information about their neuromuscular structures and communication sides that have not been previously experimentally identified.

Results

Conserved venom gland structure across coleoid lineages

To determine if there are differences in the venom secreting tissue across coleoids, we performed morphological characterization of the venom gland (PSGs) in octopus (*O. bimaculoides*), squid (*E. berryi*) and cuttlefish (*A. bandense*) specimens. Tissue micro-computed tomography (micro-CT, histotomography) reconstructions of the PSG in an *O. bimaculoides* hatchling indicate two differentiated tubule types distinguished by morphology and clear differences in texture (Fig. S2). The two types present correspond to secretory and smooth-striated tubules, as previously alluded to (10,14,15) (Fig. 1c,d). Herein, proximal-striated tubule refers to those in proximity to the posterior salivary duct (PSD), and the distal-secretory tubule are distal to the PSD (Fig. 1b-e and Fig. S2). Interestingly the micro-CT reconstruction of the PSG in *E. berryi* allowed the identification of proximal-striated tubules but challenged the identification of secretory tubules, which are shown prominently in *E. berryi* tetrachrome staining (Fig. 1e and Fig. 2e,f). Additional hematoxylin and eosin staining revealed a consistent branching architecture of numerous small tubular structures (100 – 150 µm) with heterogenous diameters and lumen sizes in *O. bimaculoides* and *D. pealeii* PSG, illuminating the differentiation between the described tubule types (Fig. 2a-d). Tetrachrome staining of PSG sections in *E. berryi* further display granules, high protein content, and distinctive tissue layers between tubules potentially involving mucopolysaccharids (Fig. 2e,f). Our findings align with previous histological descriptions of the PSGs in the common cuttlefish (*S. officinalis*) (16) and the common octopus (*Octopus vulgaris*) (17). On a cellular level, transmission electron microscopy (TEM) images confirm an affluence of secretory granules and mitochondria in the secretory epithelial cells of *E. berryi*, *O. bimaculoides* and *A. bandense* (Fig. 2g-i). Taken together, the general morphology of venom glands across coleoid taxa is consistent in tubular distribution and structure, with few differences on a cellular- level such as abundance of secretory granular and

135 mitochondria, which may vary based on different lineages, their stage of development, the venom
136 release mechanism, the position within the gland or type of tubule.

137 ***Neuro(muscular) structures and communication sites throughout coleoid venom glands***

138 To determine if venom release is an actively regulated physiological process integrated with the
139 nervous system, or a purely glandular phenomenon we characterized the muscular and/or
140 neuromuscular structures in coleoid venom glands of *O. bimaculoides* and *D. pealeii* we used
141 phalloidin and α-actin staining, respectively. Phalloidin highlights mostly the polymeric-filamentous
142 state of actin in the venom gland, while the α-actin isoform is commonly associated with smooth
143 muscle in vascular and visceral tissue. Our findings revealed an abundance of muscle fibers in *O.*
144 *bimaculoides* that were specific and localized around tubules, matching DAPI-stained cell body
145 aggregation (Fig. 3a). The α-actin staining in *D. pealeii* is strongly co-localized with the expression
146 of co-stained venom protein SE-cephalotoxin-1 (*ctx-1*) and close to the basal membrane of gland
147 tubular structure when contextualized with pkh26 membrane marker (Fig. 3b). Integration of the
148 filamentous and α-actin stains with the spatial context of the gland structure provides molecular
149 evidence for the presence of proposed circular smooth muscle layer around the secretory/striated
150 tubules as observed morphologically in octopus PSG (10). Immunohistochemical staining with SMI-
151 31 antibody targeting the heavy chains of neurofilaments, common structural elements found in
152 axons and dendrites of nerves, molecularly validated the dense axonal infiltration previously
153 described only in octopus (10,18) and now confirmed for the gland in *D. pealeii* (Fig. 3c). In addition,
154 NeuN staining - marking mature neuron nuclei and perinuclear cytoplasm - in the PSG tissue
155 sections of *A. bandense* is prominent as small, round clusters near the peripheral tubular openings
156 and extends between the tubular structures until the center of the gland, with luminal areas devoid
157 of staining (Fig. S3a). Similarly, in *D. pealeii* PSG, darkly stained round structures at the gland
158 periphery suggest Nissl bodies – large aggregates of endoplasmic reticulum and ribosomes – are
159 present in neuronal somas whose high rRNA content was targeted (Fig. S3b). While additional
160 markers are needed to distinguish neuronal from secretory cell-related expression, these findings
161 elucidate the presence of muscular and neuromuscular structures and neuronal communication
162 sites in coleoid venom glands.

163 ***Network of neuronal agents reveals potential operating routes from the nerves to venom***
164 ***release***

165 To identify potential neuronal pathways in cephalopod venom release, we assessed the synaptic
166 organization between neuronal and muscular tissue within the PSGs of squid (*E. berryi*, *D. pealeii*)
167 and octopus (*O. bimaculoides*) by mapping the spatial distribution of presynaptic vesicle-associated
168 phosphoproteins (synapsin), which participate in neurotransmitter release (19) (Fig. 3). Synapsin
169 staining in *A. bandense* tentacles confirmed marker specificity and revealed strong central and
170 peripheral signals consistent with known neuronal bundles and epidermal innervation (Fig. 3d). The
171 synapsin signals detected in octopus and squid PSGs were widespread around the tubular
172 structures, aligning with densely clustered cell nuclei with no luminal staining (Fig. 3e-h).
173 Throughout the taxa examined, synapsin distribution is congruent with actin patterns, with sharpest,
174 punctual staining in the tubular periphery of the venom gland in *O. bimaculoides* and *D. pealeii*
175 (Fig. 3f-h).
176 To characterize the postsynaptic receptors, we examined muscle-type α-nicotinic acetylcholine
177 receptors (nAChRs), which are abundant at neuromuscular junctions (NMJs), using the snake
178 venom neurotoxin, α-bungarotoxin that binds with high affinity to muscle nAChRs and with low
179 affinity to certain neuronal nAChRs (20). We confirmed staining specificity in *S. officinalis* arm
180 suckers (Fig. 3i-j), observing sharp peripheral staining where NMJs are present. In the PSGs of
181 cuttlefish (*S. officinalis* and *A. bandense*), we detected α-nAChRs in the gland periphery and diffuse
182 staining between tubular structures (Fig. 3k-n). Contextualizing the patterns obtained from these
183 single markers within the histological overview of the venom gland described above suggests that
184 the smooth muscle tissue found around the tubular system in coleoid PSGs is abundantly targeted
185 by neuronal tissue including cholinergic neurons.

186 Using hybridization chain reaction (HCR), we mapped the expression of choline acetyltransferase
187 (ChAT), which is essential for acetylcholine production in cholinergic neurons and NMJs, in squid
188 *D. pealeii* PSG. We found that the expression appears higher at the periphery of the PSG, and less
189 intense throughout the gland (Fig. 3o). To determine if ChAT expression correlated with venom
190 gene expression, probes for *D. pealeii* SE-cephalotoxin-2 (*ctx-2*) sequences were used to visualize
191 this highly expressed venom transcript in the gland sections along with cell nuclei (DAPI). While
192 ChAT expression supports the presence of acetylcholine-producing motor neurons, single-channel
193 recordings showed limited differentiation between *ctx-2* and ChAT patterns, which may indicate
194 proximity in the expression of venom protein *ctx-2* and cholinergic neurons (Fig. 3o). We repeated
195 this experiment in *O. bimaculoides* PSG, with ChAT probe and DAPI only, as SE-cephalotoxin-like
196 proteins have not been found in *O. bimaculoides* (21) (Fig. 3p). The results are comparable to the
197 ones obtained for *D. pealeii,* but with lower intensity for ChAT expression. Taken together, these
198 results provide robust evidence of a network of neuronal components that can act in concert to
199 facilitate venom release from coleoid PSGs.

200 ***Acetylcholine and dopamine-gated channels are present in coleoid venom glands***

201 To identify neuronal ion channel family diversity in the PSGs of coleoid cephalopods, we retrieved
202 cys-loop ligand-gated ion channels (cys-loop LGICs) sequences, including isoforms, from the PSG
203 transcriptomes from *O. bimaculoides*, *D. pealeii*, and *A. bandense*, and performed a comparative
204 phylogenetic analysis with other metazoan phyla. This allowed us to categorize the PSG sequences
205 and predict their functional properties. The tree was split into three major families (Fig. 4): nicotinic
206 ACh-like which are mainly cationic, GABA-A-like which are mainly anionic and cys-less which has
207 an unknown function (22).
208 GABA-A-like channels associated with anionic activity are shown on the top half of the tree (Fig 4).
209 We identified a total of 46 sequences from which 3 sequences were found in the GABA-A group.
210 We identified a cephalopod-specific subfamily (PSG unknown 1) with 11 PSG sequences from
211 *A. bandense*, which is a sister to a glutamate-gated chloride channel group from platyhelminths
212 (23). Interestingly, we also identified another cephalopod-specific group (PSG unknown 2), with 32
213 sequences from all three cephalopod species, which is sister to glutamate-gated chloride channels
214 from molluscs (24). Further characterisation is needed to determine the functional properties of
215 these anionic 'unknown' groups. Glycinergic cys-loop LGICs are present in vertebrates and
216 annelids (25), but we didn't see any evidence for these channels in cephalopods in this analysis.
217 Nicotinic acetylcholine-like channels associated with cationic activity are on the bottom of the tree
218 (Fig. 4). We identified a total of 84 sequences from octopus, squid, and cuttlefish species, of which
219 26 sequences fall within the metazoan nicotinic acetylcholine-gated channel group. We also found
220 in all three taxa of cephalopods tested, 34 sequences in the dopamine-gated channel group, which
221 was recently functionally characterised in *O. vulgaris* and other invertebrates (26). There were also
222 four groups with unknown functional properties (PSG unknown 3-6). The PSG unknown groups 4
223 and 5 were recovered as sister to the inhibitory acetylcholine receptor group B, while the PSG
224 unknown group 6 is sister to a clade comprising the dopamine-gated channels and vertebrate α9/10
225 acetylcholine gated channels. The PSG unknown 3 group is of particular interest as it is recovered
226 as sister to Cephalopod chemotactile receptors (27), which in the context of chemotactile stimuli
227 from the arms could be involved in signal transduction for venom release in the PSG. Chemotactile-
228 induced versus other forms of release of venom is an ongoing area of exploration in our group
229 requiring further investigation. In contrast, the anionic acetylcholine receptor group previously found
230 in molluscs (26,28) and the serotonin-gated channel group present in vertebrates and nematodes
231 (29), were absent in PSG sequences and likely not present in cephalopod venom glands. These
232 findings provide initial molecular and functional characterization of the ion channels found in squid,
233 cuttlefish and octopus venom glands.

234 ***Live staining of squid venom gland explant suggests calcium signaling activation***

235 To monitor neuronal signal transmission, we examined if calcium signaling could be recorded in *ex*
236 *vivo* cephalopod venom glands. Specifically, we incubated explanted PSGs from *E. berryi*, with a
237 cell-permeable fluorogenic calcium indicator. Calcium plays a versatile role in the nervous system,

but also in muscular tissue, acting as a second messenger and facilitating presynaptic exocytosis, postsynaptic signaling, and action potential development (30,31). We observed spontaneous calcium activity, particularly in areas surrounding nuclei near the edge of the PSG (Fig. 3q,r; see Movie S1). We also observed waves of calcium activity in thin processes travelling between these regions. Further analyses are required to determine if this activity is neural or muscular, and to identify the neurotransmitters or neuromodulators involved. While our *ex vivo* analysis is a pilot study, it indicates our ability to detect and measure signaling pathway activation and modulation in a real-time live staining of cephalopod venom gland explants, a previously unreported finding.

Discussion

Coleoid cephalopods (octopuses, squids, and cuttlefish) use venoms to immobilize prey, however the mechanism(s) of venom secretion is unknown. Here, we combine multimodal histological profiling and gene expression analyses with calcium activity imaging and ion channel phylogenetics to resolve venom gland architecture, innervation patterns, and neuronal signal transduction. Our data provides comprehensive experimental evidence for the hypothesis of neuromuscular control of cephalopod venom secretion morphologically assessed by Young over 60 years ago (7,9). Our results indicate that octopuses, squids, and cuttlefish share highly conserved microanatomical components of their venom gland (PSG) (Fig. 1 & 2). As a general pattern and in congruency with previous findings in *Octopus* spp. and *S. officinalis* (14,16), the glandular structure is strongly dominated by branching tubules lined with distinctive cell types that are packed with a high content of secretory granules. These tubules have varying dimensions and luminal area sizes that are potentially dependent on tissue section orientation and apical or basal localization with respect to the transition to the PSD. While the differentiation of proximal-striated and secretory tubules described in *O. vulgaris* (7,10) were identified in our *O. bimaculoides* histological analyses and micro-CT reconstructions, these features have yet to be fully verified within squid and cuttlefish PSGs. Tissue staining results in these lineages indicate a large proportion of secretory tubules but tubular differentiation within the micro-CT of *E. berryi* has been inconclusive. Further, the tandem usage of H&E and tetrachrome staining, and TEM for gland structure characterization highly support (chemical) content differentiation in the tubules (Fig. 2 & S2) but needs further optimization in the context of large PSG enzymatic content and species-specific tissue fixation success (see supplements, Fig. S4). However, the suggested differentiation observed in our findings alludes to distinct functions for parts of the tubular system with distal secretory tubules representing the production sites and the proximal smooth-striated tubule collect and propel the venom towards the salivary duct, underscoring a potential muscle-driven mechanism for venom release.

The infiltration of the venom gland by a connectivity tissue matrix enclosing blood vessels in proximity of muscle fibers targeted by nerve endings has been morphologically proposed and shown recently in single species of octopus and cuttlefish (14,16). However, a molecular verification across coleoid representatives has not been reported. Our muscular evidence identifies a high abundance of α-actin commonly found in smooth muscle fibers across the PSG of *D. pealeii* and the actin forms filamentous polymers in the PSG of *O. bimaculoides*. This matches the morphological observations from Young (7) and House (10) of circular layer of smooth muscle around the tubules in the PSG of *O. vulgaris.*

Another novel finding of muscular cholinergic receptors in the PSG of cuttlefish around the tubules match the patterns obtained from neuronal presynaptic vesicles and define clear neuromuscular communication sites in the proximity of the basal membrane of the gland tubular system. Together with the first indicators for presynaptic choline acetyltransferase signals in *D. pealeii* and *O. bimaculoides*, we present strong evidence that acetylcholine is a major neurotransmitter regulating the venom gland in cephalopods. This gains further support by our phylogenetic results indicating that fast excitatory cholinergic and dopaminergic signalling is likely playing an important role in the PSG, due to the presence of nicotinic acetylcholine and dopamine-gated channels. We also ruled out the possibility of fast cholinergic inhibition via AChRB channels, which were recently found to play a role in the *O. vulgaris* optic lobe (26). In addition, GABA and glutamatergic signalling may be acting as fast inhibitory signals, however more work is needed to confirm this. The other

290 unknown groups represent interesting avenues for further exploration and may involve novel
291 signalling mechanisms, especially in the context of chemotactile signal integration.
292 Current proposals for venom release include apocrine secretion, which involves budding of cellular
293 cytoplasm, and is typical for mammalian salivary glands (32). However holocrine secretion, which
294 involves bursting of cells, is proposed for molluscan cone snails (33). While the venom secretion
295 mechanism of no venomous snail or cephalopod is known, the neural, neuromuscular and muscular
296 structure we describe here support the hypothesis of neuromuscular control of the PSG in
297 cephalopods, with muscle fibers around the secretory tubules and a marked innervation pattern
298 across the gland. Our neuronal and neuromuscular recordings provide the first comparative insights
299 into the interplay between neuronal and glandular systems in cephalopods, a significant first step
300 in delineating the mechanisms of their brain-bite neural circuit for venom release. Similar
301 observations of neural innervation in spiders (34), scorpions (35), snakes (36) and the giant
302 centipede (37) venom glands point to a widespread phenomenon of neuronal control of venom
303 release throughout vertebrates and invertebrates but with different complexity and molecular key
304 players.
305 Together, these findings provide a multimodal foundation for interspecific comparisons of coleoid
306 venom gland architecture, from the tubular differentiation to neuromuscular networks. By resolving
307 the molecular identity of smooth muscle fibers, axonal infiltration, cholinergic neuromuscular
308 contacts, and potential calcium-dependent secretory pathways, our study clarifies how an external
309 (chemotactile) stimuli may be integrated through the superior buccal lobe and translated into the
310 activation of the secretory tubules. A cohesive working model for the transport of venom through
311 the salivary ducts toward the buccal mass may occur by activation of the secretory tubules via
312 cholinergic and dopaminergic channels, coupled with contraction of the surrounding smooth
313 muscle.
314 Whether through pioneering work on the discovery of the squid giant axon by John Z. Young (38),
315 or Alan Hodgkin and Andrew Huxley's (39) use of the squid giant axon to characterize the
316 mechanism of action potentials, the Cephalopoda nervous system has been used to advance
317 groundbreaking knowledge. Our efforts are to bring to light the cephalopod neuronal and venom
318 gland connection, which can be used to identify new circuits for animal predation, defense, and
319 sexual competition. Our approach of integrating diverse datasets of histology, computed
320 tomography models, phylogenetics and *ex vivo* calcium imaging harbors tremendous versatility for
321 future studies in tracing neuronal routes from signal integration centers to specific venom gland
322 structures, to characterize the molecular signaling networks and mechanistic sequence of
323 cephalopod venom release. As such, these approaches deepen our understanding of
324 neurosecretory systems in non-traditional model systems and hold considerable promises for
325 expanding our understanding of cephalopod biology and accelerating biodiscovery within these
326 evolutionary rich but underexplored lineages.

327 **Materials and Methods**

328 ***Animals and Tissue processing***

329 Animal specimens were obtained from the Marine Biological Laboratory, Woods Hole (MA, USA).
330 Euthanasia was performed by gradually increasing ethanol concentration from 0 to 30% in natural
331 sea water over 30 min. If not otherwise stated in the following method protocols, for all tissue section
332 staining, the PSGs from adult *D. pealeii*, *E. berryi*, *A. bandense*, *S. officinalis*, and *O. bimaculoides*
333 were dissected and processed as described below. Briefly, after dissection, the gland samples
334 were fixed overnight (at least 16 h) in 4% paraformaldehyde (PFA) in artificial salt water at 4°C.
335 Fixed samples were washed with DEPC-treated PBS and gradually dehydrated through a
336 progressive series of ethanol, of 10% increase per 20-min steps, up to 100%. To prepare the
337 tissues for embedding, samples were cleared with two changes of histosol (30 min each), followed
338 by incubation in two 1:1 histosol:paraffin solution changes (30 min each) and subsequent
339 incubation in pure paraffin overnight at 60°C. The samples underwent four to five changes in 100%
340 paraffin, each lasting 1 h, before being transferred into sectioning molds for solidification. Paraffin
341 blocks were sectioned at 8-10 µm thickness using a microtome. For RNA-hybridization

experiments, all water and phosphate buffered saline (PBS) solutions were treated with diethylpyrocarbonate (DEPC) overnight and autoclaved before use to eliminate RNase activity.

(Immuno)histochemistry

Tissue staining procedures are described in brief below; detailed protocols are available in the Supplementary Material.

a. Hematoxylin and Eosin staining. For staining, tissue sections were deparaffinized in xylene rehydrated through a descending ethanol series and subsequently stained in Harris hematoxylin (Cat.-No. HHS32, Sigma-Aldrich, Missouri, USA) and counterstained with eosin Y solution (0.5–1%; Cat.No. 611815000, ThermoScientific, Waltham, USA). Tissue slides were mounted with DPX resin.
b. Tetrachrome staining. Tetrachrome staining procedure was performed according to the protocol established by Costa and Costa (40). This protocol involves sequential staining in four different dyes: Alcian Blue 8GX (Cat.-No. A5268, Sigma-Aldrich), Periodic acid (Cat.-No. 29922, Chem Impex), Schiff's Reagent (Cat.-No. 3952016, Sigma Aldrich), Weigert's Iron Hematoxylin (Cat.-No. 1.15973, Sigma Aldrich), and aqueous Picric acid (Cat.-No. 19552, Electron Microscope Sciences, Hatfield, USA). After concluding the staining procedure, slides were dehydrated with a progressive series of ethanol, cleared with xylene and mounted in DPX resin.
c. Filamentous Actin. Tissue section were stained with phalloidin (Alexa Fluor 647, Cat.-No. 8940, Cell Signaling Technology, MA, USA), counterstained with 4',6-diamidino-2-phenylindole, dilactate (DAPI), mounted with hard-set mounting medium and coverslips. Fluorescence was recorded at 405 nm and 640 nm.
d. Neurofilament-H. Tissue sections were cleared with histosol and rehydrated through a descending ethanol series. Then, antigen retrieval and blocking was performed by using SMI-31 (Cat.-No. NE 1022, Sigma Aldrich) as primary and Donkey anti-Mouse IgG (H+L) Alexa 647 (Cat.-No. AP192SA6, Sigma Aldrich) as secondary antibody. Sections were mounted in DAPI-Fluoromount-G and coverslipped. Mounted slides were cured for approximately 24 h at 5°C before imaging. Fluorescence was recorded at 405 nm and 640 nm.
e. Alpha-Pan Actin, Membrane and Cephalotoxin-1 multiplex experiment. This involved immunohistochemistry (IHC), RNA-*in situ* hybridization chain reaction (HCR) and a membrane linker. Tissue sections were processed by a stepwise multiplexing strategy described in detail in the supplementary material. Briefly, first, the initial steps of the HCR protocol targeting cephalotoxin-1 were performed, beginning with deparaffinization, rehydration, and permeabilization (detailed below). To prevent heat-induced degradation or loss of integrity of the RNA probes used during HCR, the heat-based antigen retrieval of the IHC for the anti-pan actin antibody (Cat.-No. ab119952, Abcam, Waltham, USA) as primary antibody was carried out after these initial HCR steps. Following antigen retrieval, the HCR procedure was completed, including probe and amplifier hybridization. IHC staining was then concluded, starting from the blocking phase and followed by incubation with primary and using the Donkey anti-Mouse IgG (H+L) Alexa 647 (Cat.-No. AP192SA6, Sigma Aldrich) as secondary antibody. The multiplexing workflow was finalized through the addition of the pkh26 cell membrane labelling (Cat.-No. MIDI26, Sigma Aldrich), after which a nuclear counterstain was performed by mounting the tissue slides with DAPI-Fluoromount-G medium and finally slides were coverslipped. Fluorescence was recorded at 405 nm (DAPI), 488 nm (ctx-1), 561 nm (pkh26) and 640 nm (pan-actin).
f. Synapsin. Herein, we used an anti-SYNORF1 antibody (Cat.-No. 3C11, Developmental Studies Hybridoma Bank) that recognizes synapsin-1. This antibody is derived from the peptide sequence LFGGMEVCGL, located within the conserved C domain of synapsins. Its specificity has been validated across multiple species, including cephalopods. The secondary antibody was a goat anti-mouse IgG purchased from ThermoFisher (DyLightTM 650). The experimental

391 method followed the antigen retrieval and blocking as described by Rees et al. (41), with few
392 modifications to suit the objectives of this study. Finally, the slides were mounted in DAPI-
393 Fluoromount-G, coverslipped, and stored at 5°C and left to dry for approximately 24 h before
394 imaging. Fluorescence was recorded at 405 nm and 640 nm.

395 g. Visualization of nAChRs at Neuromuscular Junctions. We used α-bungarotoxin conjugates (Cat.
396 No. B35450, ThermoFisher) to label nAChRs and visualize neuromuscular junctions. α-
397 Bungarotoxin, a peptide derived from snake venom, binds irreversibly and with high specificity
398 to the subunit alpha of the nAChRs in muscular tissue, but has also been shown to bind with
399 lower affinity to nAChRs in the vertebrate brain (42), making it a valuable tool for their
400 visualization in situ. The rehydration, antigen retrieval, and blocking stages followed the same
401 protocol as of the synapsin. Fluorescence was recorded at 405 nm and 640 nm.

402 h. NeuN. Here, we used a Chromagenic DAB (ab64238; Abcam) staining to detect the presence
403 of neuronal nuclei with the primary NeuN antibody (ABN91; Merck Millipore) by a standard IHC
404 protocol including deparaffinization of tissue slides with xylene, antigen retrieval, and blocking
405 phases. Donkey Anit-Chicken IgY (H&L) (Cat.No. 703-065-155, Jackson ImmunoResearch,
406 West Grove, USa) was used as secondary antibody.

407 i. Nissl bodies. Squid PSG sections were used to perform a Cresyl Violet Stain (ab246817;
408 Abcam). The slide first underwent deparaffinization and rehydration before proceeding with the
409 Cresyl Violet Stain. The slide was then incubated in xylene before being cover slipped with
410 CytoSeal XYL overnight.

411 j. Choline Acetyltransferase and Cephalotoxin-2. The method was initially developed by Choi et
412 al. (43) with modifications according to Criswell and Gillis (44), and followed here accordingly.
413 Hybridization chain reaction (HCR) reagents were obtained from Molecular Instruments Inc. (LA,
414 USA), where probes for the venom protein cephalotoxin-2 for *D. pealeii* were further specifically
415 designed. The probes for choline acetyltransferase were previously designed for *Octopus bocki*
416 (45), and here tested on *D. pealeii* PSG sections. Sequences upon which the hybridized probes
417 were designed can be found in the supplemental Data S1, while the comparative alignment of
418 the *O. bocki* homolog ChAT sequences from *D. pealeii*, *O. bimaculoides and A. bandense* can
419 be found in the supplementary methods and Fig. S5, while the ChAT cephalopod homolog
420 sequences are found in Dataset S1. Fluorescence was recorded at 405 nm (DAPI), 488 nm
421 (ctx-2) and 640 nm (ChAT).

422 k. Live calcium signaling. PSG was dissected from *E. berryi* specimen immediately after
423 euthanasia and placed in a petri dish with a cephalopod-specific cell culture medium, herein
424 called octomedia (see supplements for recipe). PSGs were incubated in the calcium indicator
425 CAL-520 (Cat.-No. ab171868, Abcam, UK) that is known to improve signal-to-noise ratios
426 compared to standard calcium imaging, allowing live fluorescence recordings of calcium
427 migration within the PSG (46). Imaging was performed with an upright epifluorescent
428 microscope equipped with a 490/525 nm excitation/emission filter set and operated at 2fps.
429 Calcium imaging videos were processed as follows: image registration was performed within
430 suite2p using the non-rigid registration approach (47), spontaneously active regions were
431 manually defined, normalised using a min/max approach and plotted using a custom python
432 script. The maximum intensity projection image shown in Fig. 3 was prepared for publication
433 using ImageJ (48).

434 ***Microscopy and Image Processing***

435 Several different imaging techniques were employed to visualize the models, histological details,
436 and staining results.

437 a. Electron Transmission Microscopy. Samples were washed with PBS, then fixed with a modified
438 Karnovsky's fix of 2.5% glutaraldehyde, 4% PFA and 0.02% picric acid in 0.1M sodium
439 caocdylate buffer at pH 7.2 (49). Following a secondary fixation in 1% osmium tetroxide, 1.5%

potassium ferricyanide, samples were dehydrated through a graded ethanol series, and embedded in an epon analog resin. Ultrathin sections were cut using a Diatome diamond knife (Diatome, USA, Hatfield, PA) on a Leica EMEC7 ultramicrotome (Leica, Vienna, Austria). Sections were collected on copper grids and contrasted with lead citrate (50) and viewed on a JEM transmission 1400 electron microscope (JEOL, USA, Inc., Peabody, MA) operated at 100 kV. Images were recorded with a Veleta 2K x2K digital camera using RADIUS software (EMSIS, Germany).

b. Micro-Computer Tomography. An *O. bimaculoides* hatchling was obtained from the Marine Biological Laboratory and anesthetized in sea water with several percent ethanol and placed in a fixative of 4% paraformaldehyde in sea water for several days. The hatchling was immersed for a week in phosphotungstic acid and eosin solution, rinsed several times with distilled water, and then chemically dehydrated with acidified 2-2-di-methoxypropane (DMP) overnight. It was then immersed in hexamethyl di-silazane (HDMS) and air dried overnight in a hood. The intact animal was glued to an aluminium SEM stub mounted with plasticine onto a ThorLabs half inch diameter optical post screwed into a 1x1" kinematic base for imaging.

   Parallel beam synchrotron X-ray imaging was performed at sector 2 bending magnet beamline (2BM) of the Advanced Photon Source (APS) of Argonne National Laboratory. The beam energy was monochromatic and set to 25.5 keV and a sample to scintillator distance of 70 mm was used. Two sets of 9001 X-ray projections were collected over 360° of sample rotation to reconstruct the hatchling. 28% overlap between tomograms was chosen to minimize stitching artifact. Each projection was captured using a custom wide-field detector and camera with a 10mm field-of-view (FOV) and 0.7 μm^4 voxel size. The 3D reconstructions were calculated using the gridrec algorithm from TomoPy (51) and stitched with manual alignment in ImageJ. The Bronnikov Aided Correction was used for phase retrieval with alpha and beta parameters equal to 2.0 (52,53).

   A formalin-fixed, paraffin-embedded *E. berryi* sepiolid squid was obtained from the Rosenthal Lab at the Marine Biological laboratory. Excess paraffin was removed via scalpel and excess paraffin wax was used to affix the sample to a plastic sample holder. Parallel beam synchrotron X-ray imaging was performed at beamline 8.3.2 of the Advanced Light Source (ALS) of Lawrence Berkeley National Laboratory. The beam energy was monochromatic and set to 14 keV, and a sample to scintillator distance of 50 mm was used. 1969 projections with 300 ms of exposure time were captured over 180 degrees of rotation using a 5 mm FOV detector with 0.5 µm isotropic voxel size. The 3D reconstructions were calculated using the gridrec algorithm from TomoPy and stitched with manual alignment in ImageJ. The Bronnikov Aided Correction was used for phase retrieval with alpha and beta parameters equal to 2.0 and 1.25 respectively (52,53).

c. Confocal microscopy. The imaging of the phalloidin, SMI-31, multiplexed experiment, synorf-1 (Fig. 3d-g), NMJ and ChAT were performed using a Zeiss LSM 880 confocal microscope equipped with 10x, 25x, 40x, and 63x objectives. Image processing was performed with the Zeiss Zen 3.10 blue version and ImageJ software.

d. Light microscopy. Synorf-1 staining in *D. pealeii* (Fig. 3h) was captured with a Zeiss Axioscope 5 at a resolution of 1024 × 1024 pixels. Images were processed with Image J Fiji software.

e. Digital Slide scan. Tetrachrome and H&E tissue slides were scanned at 40× using an Aperio AT2 slide scanner (Leica Biosystems, Nussloch, Germany) and images were saved in TIFF format. Image processing was made with the manufacturer ImageScope software. NeuN and Nissl body stainings were visualized on a digital pathology scanner (NanoZoomer-SQ Digital slide scanner, Hamamatsu Photonics K.K., Shizuoka, Japan).

Comparative phylogenetic analysis of metazoan cys-loop LGICs

We used the 'cys-loop' LGIC dataset from Courtney *et al.* (26) which included 26 species of metazoans across all major phyla and 1197 sequences. We added cys-loop LGIC sequences identified from *O. bimaculoides*, *D. pealeii*, and *A. bandense* PSG transcriptomes to this dataset (see supplements for methodological details). Alignment, trimming, tree generation and visualization were performed as described in Courtney *et al.* (26). In brief, alignment was performed using MAFFT (v7.505) with E-INS-i parameters (54), trimming was performed using Trimal (v1.4.1) gappyout method (55). Phylogenies were generated using IQ-TREE v2.1.4_beta with 1,000 ultra-fast bootstraps (56). The tree model was calculated using IQ-TREE's ModelFinder implementation according to Bayesian inference criterion, and LG+F+R10 was used. The tree was visualized using TreeViewer (57). We used the cys-less group identified by Jaiteh *et al. (*22) to root the tree. The alignment of the metazoan cys-loop LGIC sequences and the phylogeny with full annotations are available as supplemental files.

Acknowledgments

The authors want to express their gratitude to the Marine Biological Laboratory's Cephalopod Breeding, which resolved the husbandry of the specific species of squids (*E. berryi* and *D. pealeii*) cuttlefish (*A. bandense* and *S. officinalis*) and octopus (*O. bimaculoides*) used in this study and thus, represents a technological springboard for the detailed study of venom biology ex situ. M.H. also acknowledges MBL Whitman Fellow Kirsten Sadler Edepli for contributions to phalloidin staining. The authors would also like to thank Roger Hanlon and Stephen Senft for contributing the *O. bimaculoides* hatchling the Cheng lab team and 2-BM beamline scientists at Argonne National Laboratory for micro-CT based histotomography, Joshua Rosenthal for the access to the *E. berryi* micro- computed tomography and Jean Cooper for assistance with the digital scanning of presented tissue sections. The authors further acknowledge the Electron Microscopy & Histology services of the Weill Cornell Medicine Microscopy and Image Analysis Core, with special thanks to Juan Jimenez for his technical assistance, as well as the Harvard Center for Biological imaging and the PAIR-UP program at Marine Biological Laboratories allowing access to cutting-edge microscopy equipment and expertise. We would like to further thank Federica Pizzulli for the contribution of her expertise to fruitful and exciting discussions on the observed patterns.

Funding

This research and the open accessibility were funded by the National Institutes of Health – Pioneer Award, grant number 5DP1AT012812 to M.H. and an E.E. Just MBL Whitman Fellowship to M.H. The accessibility to the Transmission Electron Microscope at the Weill Cornell Medicine facility was granted by a NIH Shared Instrumentation Grant (S10RR027699) for Shared Resources. Manuscript contents are solely the responsibility of the authors and do not necessarily represent the official views of the NIH. The funders had no role in study design, data collection and analysis, decision to publish or preparation of the manuscript.

Institutional Review Board Statement

The animal study protocol was approved by the Institutional Review Board (or Ethics Committee) of The Marine Biological Laboratory (protocol code 2023_MBL-IBC-36 approved June 16, 2023).

Data and materials availability

High-resolution digital scans of the *Octopus bimaculoides* hatchling and posterior salivary gland tissue sections are available at https://bio-atlas.psu.edu

535 **References**

536 1. J.A. Mather, M.J. Kuba, The cephalopod specialties: complex nervous system, learning,
537 and cognition. *Can J. Zool.* **91**, 431-449 (2013)
538 2. A.L. Allcock, A. Lindgren, J.M. Strugnell, The contribution of molecular data to our
539 understanding of cephalopod evolution and systematics: a review. J. *Nat. His.* **49,** 1373-
540 1421 (2015).
541 3. M. Holford, M. Daly, G.F. King, R.S. Norton, Venoms to the rescue. *Science* **361,** 842-844
542 (2018).
543 4. V. Schendel, L.D. Rash, R.A. Jenner, E.A. Undheim, The diversity of venom: the
544 importance of behavior and venom system morphology in understanding its ecology and
545 evolution. *Toxins* **11**, 666 (2019).
546 5. G.F. King (Ed.). Venoms to drugs: venom as a source for the development of human
547 therapeutics. *Royal Society of Chemistry* (2015).
548 6. C.B. Albertin, P.S. Katz, Evolution of cephalopod nervous systems. *Curr. Biol.* **33**, R1087-
549 R1091 (2023).
550 7. J.Z. Young, The buccal nervous system of *Octopus*. *Philos. Trans. R. Soc. Lond. B. Biol.*
551 *Sci.* **249,** 27-44 (1965).
552 8. P.J. Gibbs, P. Greenaway, Histological structure of the posterior salivary glands in the blue
553 ringed octopus *Hapalochlaena maculosa* Hoyle. *Toxicon* **16,** 59-70 (1978).
554 9. J.Z. Young, The nervous pathways for poisoning, eating and learning in *Octopus*. J. *Exp.*
555 *Biol.* **43**, 581-593 (1965).
556 10. C.R. House, Physiology of invertebrate salivary glands. *Biol. Rev.* **55,** 417-473 (1981).
557 11. J. Gorson, M. Holford, Small packages, big returns: uncovering the venom diversity of
558 small invertebrate conoidean snails. *Int. Comp. Biol.* **56,** 962-972 (2016).
559 12. F.E. Anderson, A.R. Lindgren, Phylogenomic analyses recover a clade of large-bodied
560 decapodiform cephalopods. *Mol. Phylogenet. Evol.* **156**, 107038 (2021).
561 13. R. Hanlon, M. Vecchione, L. Allcock, Octopus, Squid, and Cuttlefish: A visual, scientific
562 guide to the oceans' most advanced invertebrates. University of Chicago Press. (2018).
563 DOI: 10.7208/9780226459738
564 14. R. Anadón, "Functional Histology: The Tissues of Common Coleoid Cephalopods" in
565 Handbook of pathogens and diseases in cephalopods, C. Gestal, et al. Eds. (Springer,
566 2019), pp. 39-86.
567 15. A.I. Matus, Fine structure of the posterior salivary gland of *Eledone cirrosa* and *Octopus*
568 *vulgaris*. *Zeitschrift für Zellforschung und mikroskopische Anatomie*, **122,** 111-121 (1971).
569 16. C. Gonçalves, I. Moutinho Cabral, A.P. Alves de Matos, A.R. Grosso, P.M. Costa,
570 Transcriptome profiling of the posterior salivary glands of the cuttlefish *Sepia officinalis*
571 from the Portuguese West coast. *Front. Mar. Sci.* **11,** 1362824 (2024).
572 17. R. Fernández-Gago, P. Molist, F. Rocha, Anatomical and histochemical features of the
573 digestive system of *Octopus vulgaris* Cuvier, 1797 with a special focus on secretory cells.
574 *Acta Zool.* **100,** 320-335 (2019).
575 18. R. Martin, J. Barlow, Localisation of monoamines in nerves of the posterior salivary gland
576 and salivary centre in the brain of Octopus. Zeitschrift für Zellforschung und
577 mikroskopische Anatomie, **125**, 16-30 (1972).
578 19. B.R. Klagges, *et al.*, Invertebrate synapsins: a single gene codes for several isoforms in
579 *Drosophila. J. Neurosci.* **16,** 3154-3165 (1996).
580 20. S.M. Sine, J.R. Strikwerda, S. Mazzaferro, Structural basis for α-bungarotoxin insensitivity
581 of neuronal nicotinic acetylcholine receptors. *Neuropharma.* **160,** 107660 (2019).
582 21. P. Naidu et al., Into the Beak: Deciphering and visualizing venom expression in
583 cephalopods, *under revision.*
584 22. M. Jaiteh, A. Taly, J. Hénin, Evolution of pentameric ligand-gated ion channels: Pro-loop
585 receptors. *PloS one*, **11,** e0151934 (2016).
586 23. V. Dufour, R.N. Beech, C. Wever, J.A. Dent, T.G. Geary, Molecular cloning and
587 characterization of novel glutamate-gated chloride channel subunits from *Schistosoma*
588 *mansoni*. *PLoS pathogens*, **9.** e1003586 (2013).

24. J. Kehoe, *et al. Aplysia* cys-loop glutamate-gated chloride channels reveal convergent evolution of ligand specificity. *J. Mol. Evol.* **69,** 125-141 (2009).
25. E. Wijckmans, Functional and biochemical characterization of *Alvinella pompejana* Cys-loop receptor homologues. *Biophys.J.* **110,** 602a-603a (2016).
26. A. Courtney *et al.*, Novel dopaminergic neurotransmission in the *Octopus* visual system. *bioRxiv*, 2025-04 (2025).
27. L. van Giesen, P.B. Kilian, C.A. Allard, N.W. Bellono, Molecular basis of chemotactile sensation in octopus. *Cell*, **183,** 594-604 (2020).
28. P. van Nierop, Identification of molluscan nicotinic acetylcholine receptor (nAChR) subunits involved in formation of cation-and anion-selective nAChRs. *J. Neurosci.*, **25,** 10617-10626 (2005).
29. R. Ranganathan, S.C. Cannon, H.R. Horvitz, MOD-1 is a serotonin-gated chloride channel that modulates locomotory behaviour in *C. elegans*. *Nature* **408,** 470-475 (2000).
30. C. Grienberger, A. Konnerth, Imaging calcium in neurons. *Neuron* **73,** 862-885 (2012).
31. M.J. Berridge, P. Lipp, M.D. Bootman, The versatility and universality of calcium signalling. *Nat. Rev. Mol. Cell Biol.* **1,** 11-21 (2000).
32. R. Farkaš, Apocrine secretion: new insights into an old phenomenon. *Biochim. Biophys Acta* **1850,** 1740-1750 (2015).
33. F.J. Vonk, *et al.,* A non-lethal method for studying scorpion venom gland transcriptomes, with a review of potentially suitable taxa to which it can be applied. *PlosOne* **16,** e0258712 (2021).
34. U. Järlfors, D.S. Smith, F.E. Russell, Nerve endings in the venom gland of the spider *Latrodectus mactans*. *Toxicon* **7,** 263–264 (1969).
35. J.E. Mazurkiewicz, E.M. Bertke, Ultrastructure of the venom gland of the scorpion, *Centruroides sculpturatus* (Ewing). *J. Morphol.* **137,** 365–383 (1972).
36. C.M. Kerchove, S.M. Carneiro, R.P. Markus, N. Yamanouye, Stimulation of the α-adrenoceptor triggers the venom production cycle in the venom gland of *Bothrops jararaca*. *J. Exp. Biol.* **207,** 411–416 (2004).
37. V. Schendel, *et al.,* Exaptation of an evolutionary constraint enables behavioural control over the composition of secreted venom in a giant centipede. *Nat. Ecol. Evol.* **9,** 73–86 (2025).
38. J.Z. Young, The Functioning of the Giant Nerve Fibres of the Squid. *J. Exp. Biol*. **15,** 170-185 (1938).
39. A.L. Hodgkin, A.F. Huxley, Action potentials recorded from inside a nerve fibre. *Nature* 144, 710–711 (1939).
40. P.M. Costa, M.H. Costa, Development and application of a novel histological multichrome technique for clam histopathology. *J. Inv. Pat.* **110,** 411-414 (2012).
41. J.M. Rees, *et al.,* A pre-vertebrate endodermal origin of calcitonin-producing neuroendocrine cells. *Development* **151,** dev202821 (2024).
42. N.G. Castro, E.X. Albuquerque, alpha-Bungarotoxin-sensitive hippocampal nicotinic receptor channel has a high calcium permeability. *Biophysical J.* **68** 516-524 (1995).
43. H.M. Choi, Third-generation *in situ* hybridization chain reaction: multiplexed, quantitative, sensitive, versatile, robust. *Development* **145,** dev165753 (2018).
44. K.E. Criswell, J.A. Gillis, Resegmentation is an ancestral feature of the gnathostome vertebral skeleton. *Elife* **9,** e51696 (2020).
45. G.C. Winters-Bostwick, S.E. Giancola-Detmering, C.J. Bostwick & R.J. Crook, Three-dimensional molecular atlas highlights spatial and neurochemical complexity in the axial nerve cord of octopus arms. *Curr. Biol.*, **34,** 4756-4766 (2024).
46. M. Tada, A. Takeuchi, M. Hashizume, K. Kitamura, M. Kano, A highly sensitive fluorescent indicator dye for calcium imaging of neural activity *in vitro* and *in vivo*. *Europ. J. Neurosci.* **39,** 1720-1728 (2014).
47. M. Pachitariu, *et al.*, Suite2p: beyond 10,000 neurons with standard two-photon microscopy. *BioRxiv* 061507 (2016).
48. J. Schindelin, *et al.*, Fiji: an open-source platform for biological-image analysis. *Nat. Methods* **9**, 676–682 (2012).

49. S. Ito, Formaldehyde-glutaraldehyde fixatives containing tri nitro compounds. *J. Cell Biol.* **39,** 168A-169A (1968).
50. J.H. Venable, R. Coggeshall, A simplified lead citrate stain for use in electron microscopy. *J. Cell Biol.* **25,** 407 (1965).
51. D. Gürsoy, F. De Carlo, X. Xiao, C. Jacobsen, TomoPy: a framework for the analysis of synchrotron tomographic data. *J. Synchrotron Radiat***. 21,** 1188–1193 (2014).
52. Y. De Witte, M. Boone, J. Vlassenbroeck, M. Dierick, L. Van Hoorebeke, Bronnikov-aided correction for x-ray computed tomography. *J. Opt. Soc. Am. A* **26**, 890–894 (2009).
53. L.M. Lohse, *et al.*, A phase-retrieval toolbox for X-ray holography and tomography. *J. Synchrotron Radiat*. **27,** 852–859 (2020).
54. K. Katoh, D.M. Standley, MAFFT multiple sequence alignment software version 7: improvements in performance and usability. *Mol. Biol. Evol.* **30,** 772-780 (2013).
55. S. Capella-Gutiérrez, J.M. Silla-Martínez, T. Gabaldón, trimAl: a tool for automated alignment trimming in large-scale phylogenetic analyses. *Bioinformatics* **25,** 1972-1973 (2009).
56. B.Q. Minh, IQ-TREE 2: new models and efficient methods for phylogenetic inference in the genomic era. *Mol. Biol. Evol.* **37,** 1530-1534 (2020).
57. G. Bianchini, P. Sánchez-Baracaldo, TreeViewer: Flexible, modular software to visualise and manipulate phylogenetic trees. *Ecol. Evol.* **14,** e10873 (2024).

Figures and Tables

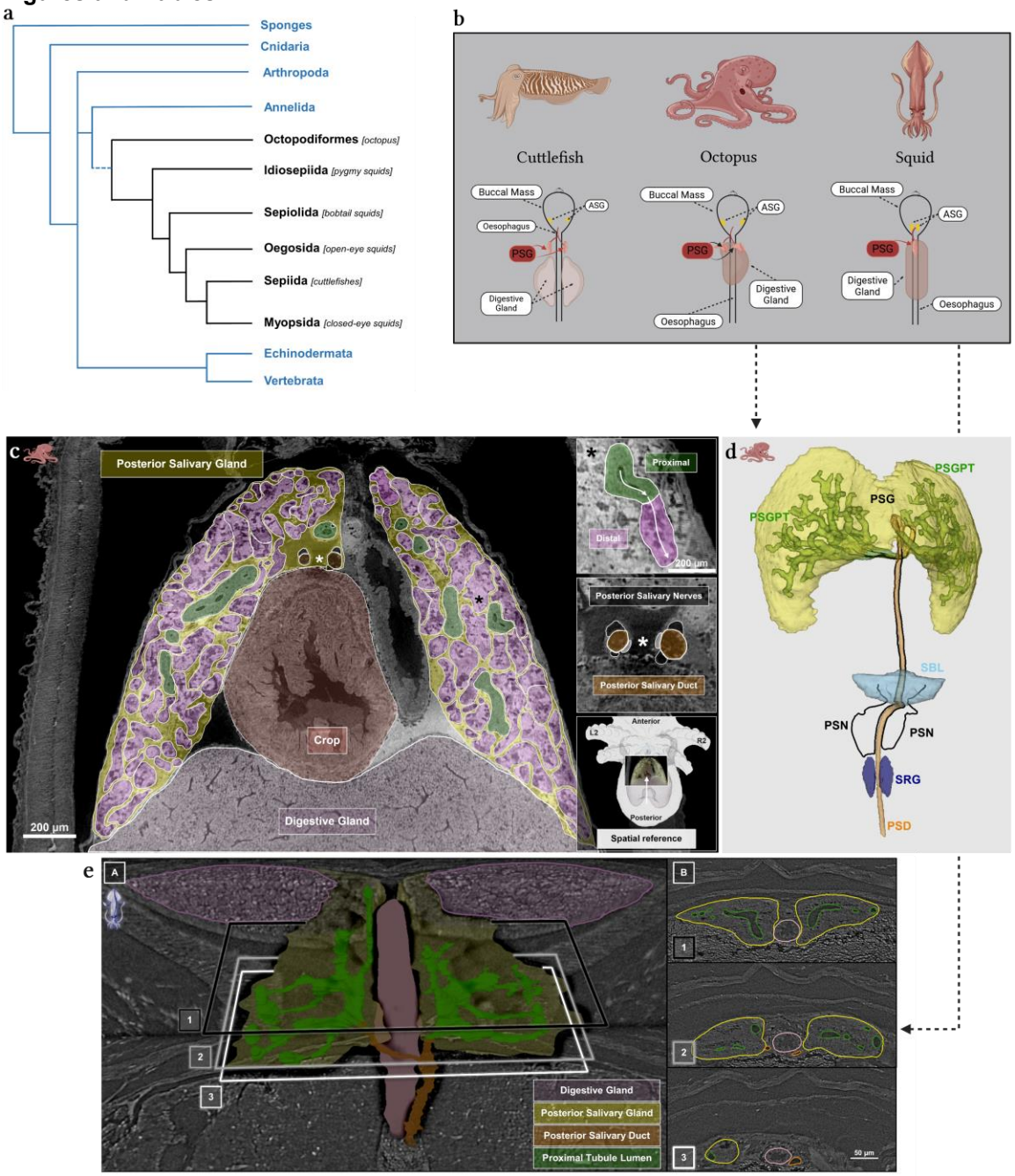

Figure 1. Cephalopods produce venom in their posterior salivary glands, which can be paired or single. a, Phylogenetic tree of venomous animal taxa highlighting the position of venomous coleoid cephalopods, *i.e.* octopuses, squids, and cuttlefish (adapted from (11,12). **b,** Anatomy of the venom system in coleoid lineages comprising the posterior salivary gland (PSG), *i.e.* venom gland (single or paired), venom duct, salivary papilla and buccal mass (dorsal view; adapted from (13) in BioRender https://BioRender.com). **c,** Micro-computed tomography (CT) 2D reconstruction of a transversal single 4 µm section of an *Octopus bimaculoides* hatchling shows the paired PSGs, proximal-striated (green) and distal-secretory (pink) tubules, posterior salivary nerves (black), posterior salivary duct (PSD) and digestive gland (purple) in corresponding color code to the 3D model in d. **d,** Micro-CT based 3D reconstruction highlights the segmentation of the gland's tubular system (PSGT; green) as well as neuronal tracing from the posterior salivary nerve fibers (PSN; black) of the superior buccal lobe (SBL; light blue) to the PSG (yellow) in *O. bimaculoides* hatchling.

677 The subradular ganglion (SRG; dark blue) and PSD are also shown. **e,** Micro-CT 2D reconstruction of a
678 transversal single 4 µm section of an *Euprymna berryi* juvenile shows the paired PSGs, proximal-striated
679 (green), PSD and digestive gland (purple).

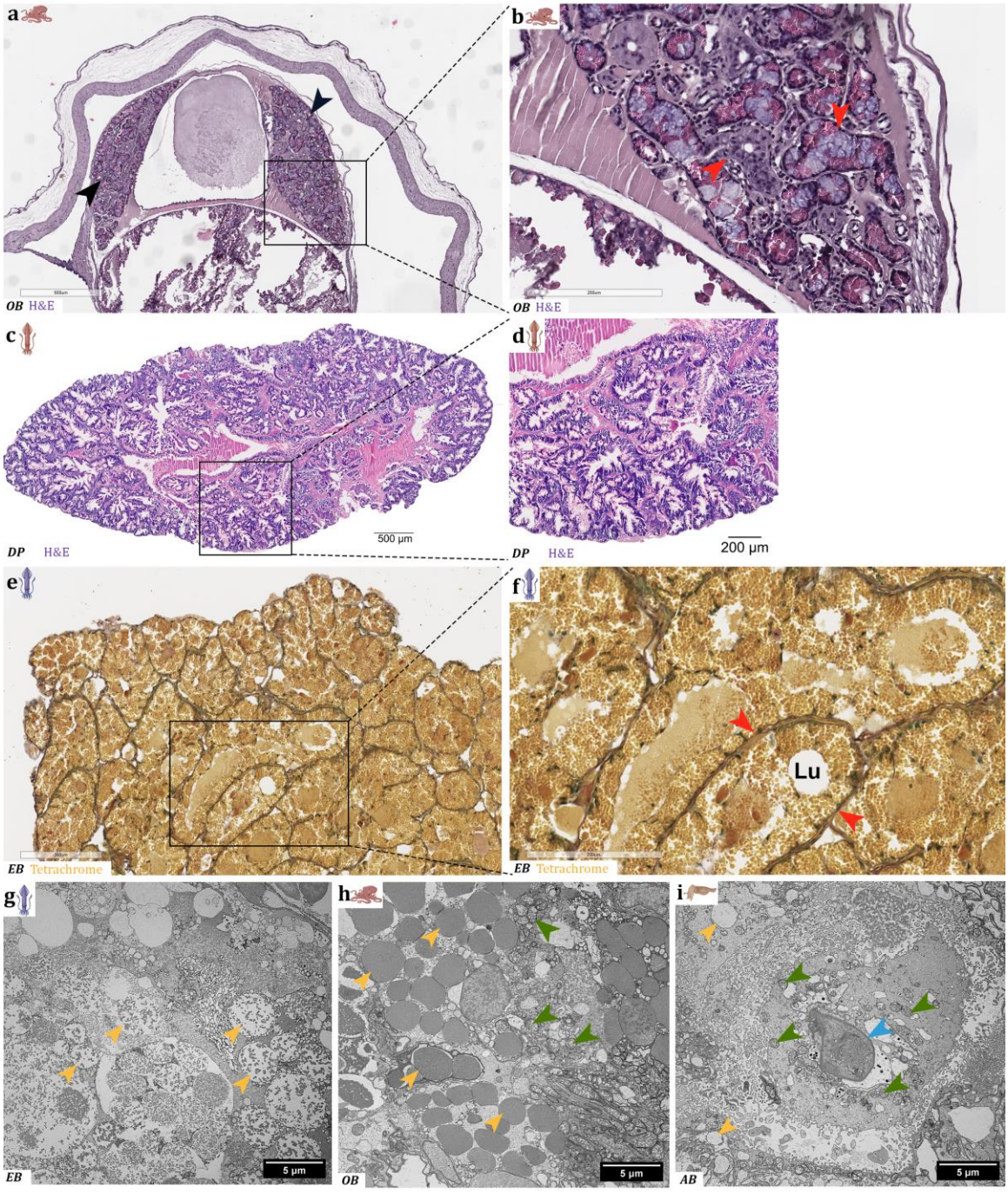

Figure 2. Histological characterization of coleoid posterior salivary glands (PSGs) reveal cross-lineage structural similarities. **a,b,** Hematoxylin and eosin staining of a formalin fixed, paraffin-embedded section of the PSG of adult *Octopus bimaculoides* and **c,d,** in *Doryteuthis pealeii*. Arrowheads: PSG (black), tubules (red). **e,f,** Tetrachrome staining in a tissue section of the PSG of an adult sepiolid squid *Euprymna berryi*. Lu = Lumen, arrowheads = tubules (red). **g-i,** Transmission electron microscopy images from the PSG of *E. berryi* (e), *O. bimaculoides* (f), and *Ascarosepion bandense* (g) highlighting abundant secretory granules and mitochondria. a-d, were obtained by high resolution digital slide scanning technique. Arrowheads: secretory granules (yellow), mitochondria (green), nucleus (blue).

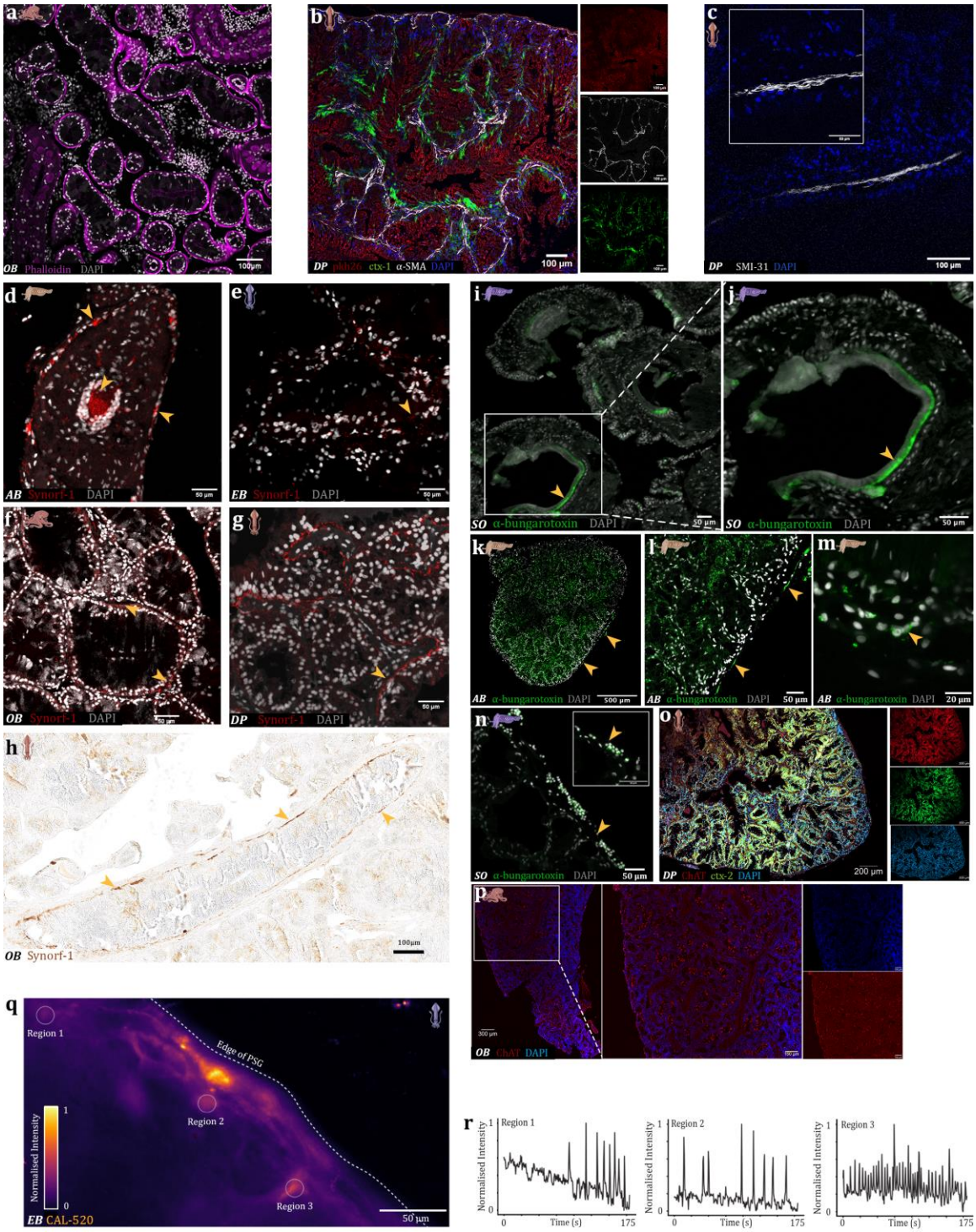

Figure 3. A network of neural agents is present in the posterior salivary glands (PSGs) of coleoid cephalopods. **a,** Muscle fiber distribution throughout the PSG in *Octopus bimaculoides* was visualized by staining actin filaments (phalloidin: purple) along with cell nuclei (DAPI: grey) for highlighting cell density distribution. **b,** Multiplexed immunohistochemistry and RNA-hybridization experiment in *Doryteuthis pealeii* PSG tissue section with the membrane cell linker pkh26 (red), alpha-actin smooth muscle marker (grey), SE-cephalotoxin-1 (*ctx-1*, green), the highly expressed venom protein in cephalopods and cell nuclei stained with

DAPI. Single channel recordings are highlighted on the right side of this panel. **c,** Heavy chain of the neurofilament (grey) found in the PSG of *D. pealeii*. **d-h,** Synapses were visualized by staining phosphoproteins known to be abundant in presynaptic cytoplasm (synapsin) along with nuclear staining (DAPI: grey) in **d,** tentacle of adult *Ascarosepion bandense* (AB); and PSG of adult **e,** *Euprymna berryi* (EB), **f,** *O. bimaculoides* (OB), and **g, h,** *D. pealeii* (DP). **i-n,** Neuromuscular junctions visualized by labeling the alpha subunit of the muscle-type nicotinic acetylcholine receptor with α-bungarotoxin (α-nAChR: green) with cell density revealed by nuclear staining (DAPI: grey) in **i, j,** arm suckers and **n,** PSG of adult *Sepia officinalis* (SO), and **k-m,** *A. bandense* under different magnification. **o,** RNA-Hybridization chain reaction targeting choline acetyltransferase (ChAT: red) and SE-cephalotoxin-2 (*ctx-2*, green) in adult *D. pealeii* PSG and **p,** ChAT expression in adult *O. bimaculoides* at larger magnification (middle) from the overview image (left), and with the single DAPI-cell nuclei stained and ChAT channel recordings (right panels). **q,** Maximum intensity projection recorded in *ex vivo* PSGs of adult *E. berryi* during calcium imaging. **r,** Mean normalized intensity over time of regions 1-3 highlighted in p. Prominent signals highlighted with yellow arrowheads. The original calcium imaging recording in the ex vivo PSG can be found in supplementary material, *i.e.* Movie S1.

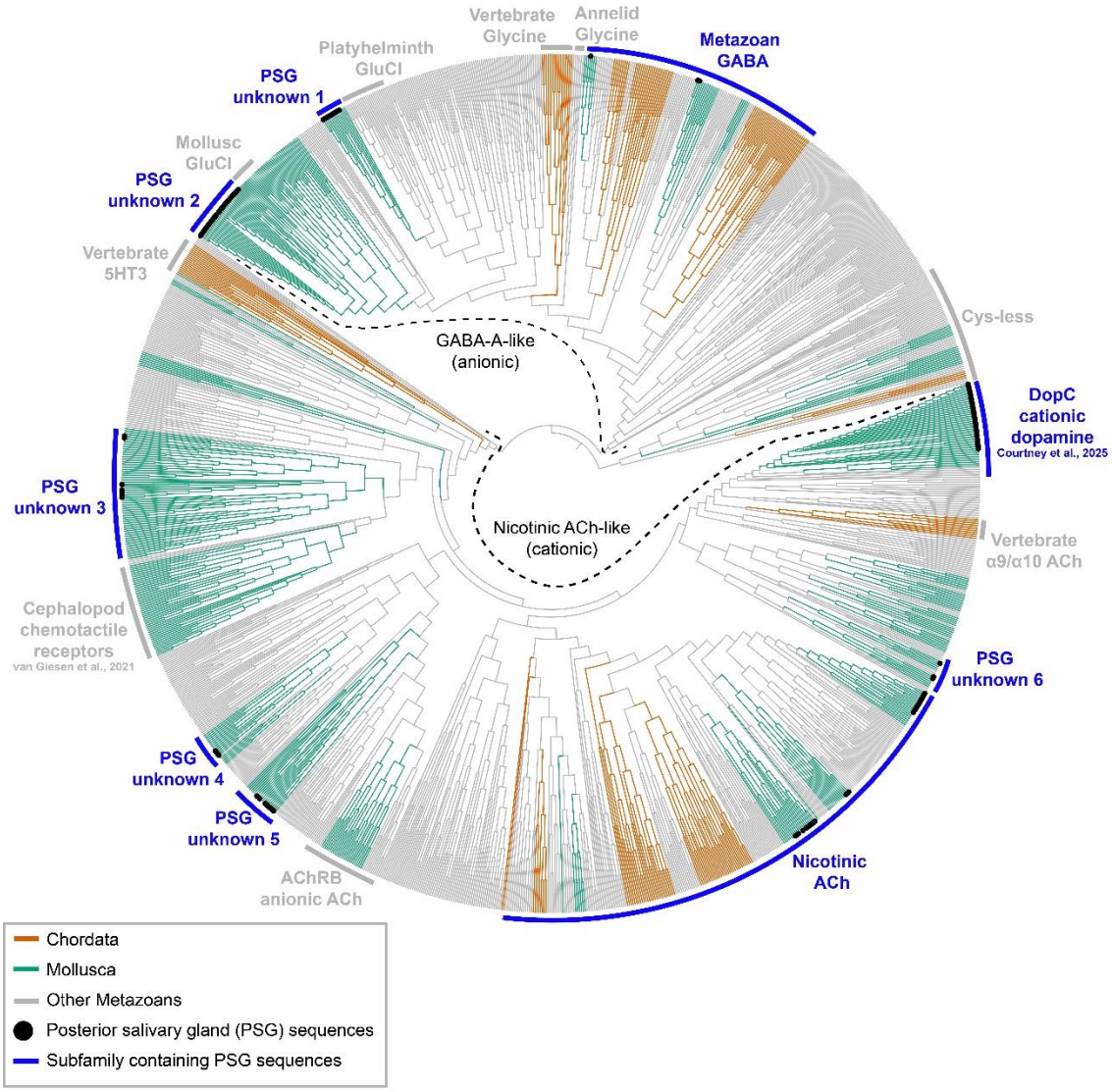

Figure 4. Comparative phylogenetics of cys-loop ligand gated ion channels from major metazoan phyla. Using venom gland (PSG) transcriptome sequences from *Octopus bimaculoides*, *Doryteuthis pealeii* and *Ascarosepion bandense* we identified excitatory acetylcholine and dopamine gated ion channels similar to those found in other metazoans. GABA-A-like channels associated with anionic activity are shown on the top half of the tree, while nACh-like channels associated with cationic activity are on the bottom. Further, several PSG sequence clusters were recovered with uncharacterized function but sister to either glutamate-gated channels (PSG unknown group 1 and 2), cephalopod chemotactile receptor group (PSG unknown 3) or inhibitory acetylcholine receptor group B (PSG unknown 4 and 5). Chordata sequences are highlighted in orange, molluscan sequences are in green, and all other metazoan sequences are in grey. PSG sequences are highlighted as black dots at the end of leaves, while subfamilies containing PSG sequences are highlighted in blue. PSG: posterior salivary gland.